corrected Proof

AQUA
Water Infrastructure, Ecosystems and Society

IWA PUBLISHING

AQUA — Water Infrastructure, Ecosystems and Society Vol 00 No 0, 1 doi: 10.2166/aqua.2024.222

Application of machine learning and statistical approaches for optimization of heavy metals (Cd^{2+}, Pb^{2+}, Cu^{2+}, and Zn^{2+}) adsorption onto carbonized char prepared from PET plastic bottle waste

Tapos Kumar Chakraborty[a,*], Md. Sozibur Rahman[a], Khandakar Rashedul Islam[a], Md. Simoon Nice[a], Baytune Nahar Netema[a], Samina Zaman[a], Gopal Chandra Ghosh[a], Md Abu Rayhan[a], Md. Jahed Hassan Khan[a], Asadullah Munna[a], Md. Muhaiminul Haque[a], Himel Bosu[a], Nazmul Hossain[b], Monishanker Halder[b] and Abu Shamim Khan[c]

[a] Department of Environmental Science and Technology, Jashore University of Science and Technology, Jashore 7408, Bangladesh
[b] Department of Computer Science and Engineering, Jashore University of Science and Technology, Jashore 7408, Bangladesh
[c] Environmental Laboratory, Asia Arsenic Network, Jashore 7400, Bangladesh
*Corresponding author. E-mail: taposchakraborty@just.edu.bd

ABSTRACT

This study focuses on the probable use of carbonized char prepared from PET plastic bottles for heavy metals (HMs) adsorption (Cd^{2+}, Pb^{2+}, Cu^{2+}, and Zn^{2+}). The prepared adsorbent is characterized by field-emission scanning electron microscopy (FE-SEM), energy dispersive X-ray spectroscopy (EDX), and Fourier-transform infrared spectroscopy (FTIR). Batch adsorption experiments were conducted with the influencing of different operational conditions: contact time (1–180 min), adsorbate concentration (25–300 mg/L), adsorbent dose (0.5–6 g/L), pH (3–7), and temperature (25–60 °C). High coefficient value [Cd^{2+} ($R^2 = 0.99$), Pb^{2+} ($R^2 = 0.97$), Cu^{2+} ($R^2 = 0.94$), and Zn^{2+} ($R^2 = 0.98$)] of process optimization model suggest that this model was significant, where pH and adsorbent dose expressively stimulus removal efficiency including 86.68, 73.66, 67.10, and 57.04% for Cd^{2+}, Pb^{2+}, Cu^{2+}, and Zn^{2+} at pH (7), respectively. Furthermore, ANN and BB-RSM revealed a good association between the tested and projected values. The maximum monolayer adsorption capacity of Cd^{2+}, Pb^{2+}, Cu^{2+}, and Zn^{2+} was 263.157, 78.740, 196.078, and 84.745 mg/g, respectively. Pseudo-second-order was the well-suited kinetics, where Langmuir and Freundlich isotherm could explain better for equilibrium adsorption data. Thermodynamic study shows HMs adsorption is favorable, exothermic, and spontaneous.

Key words: adsorption, heavy metals, machine learning methods, PET plastic waste bottle

HIGHLIGHTS

- Carbonized adsorbent was prepared from PET bottle waste by a simple thermal dissociation method.
- Response surface methodology and artificial neural network express a strong correlation between the experimental and projected heavy metal removal efficiency.
- Carbonized adsorbents reveal satisfactory results for experimental (Cd = 86.68%, Pb = 73.66%, Cu = 67.10%, and Zn = 57.04%) and real wastewater applications (Cd = 99.2%, Pb = 62.20%, Cu = 97.63%, and Zn = 64.47%).

1. INTRODUCTION

Rapid industrialization and urbanization development (e.g. diverse domestic and industrial activities) release an enormous amount of heavy metals (HMs)–containing wastewater, which finally discharges to our aquatic and terrestrial environment (Chakraborty *et al.* 2021a, 2023a; Chanda *et al.* 2021). Environmental pollution by metals and metalloids is considered a matter of global concern among researchers due to their persistent, non-biodegradability, potentially toxic character and is a severe disease creator to all living organisms via bioaccumulation and biomagnification (Al-Malack & Basaleh 2016; Ghosh *et al.* 2020a; Chakraborty *et al.* 2022a, 2022b, 2023b). Therefore, wastewater must be free from HMs before being released into the receiving environment to maintain environmental quality and develop an eco-friendly industry (Boulaiche *et al.* 2019; Chakraborty *et al.* 2021b, 2023c). Numerous treatment methods including membrane filtration, sedimentation, oxidation, nanofiltration, photo-catalytic degradation, ozonation, chemical precipitation, biological operations,

electrochemical technologies, coagulation/flocculation, solid-phase extraction, ion exchange, and adsorption have been applied for elimination of diverse pollutants (e.g. organic and inorganic) from wastewater (Ghosh *et al.* 2018, 2020b; Bhattacharjee *et al.* 2020; Zaman *et al.* 2022). Furthermore, several treatment methods are either costly or have several drawbacks (Zaman *et al.* 2022). Barakat (2011) has extensively explored the benefits and limitations of various treatment methods. Adsorption is mostly using effluent treatment techniques with aspects such as easy to operate and design, cost-effectiveness, greater performance, source availability, lower sludge production, flexibility, and insensitivity to hazardous elements (Chakraborty *et al.* 2020, 2021b). The usability of marketable activated carbon is reducing due to high cost (Zaman *et al.* 2022). In this favor, many wastes and biomaterials were used as adsorbents for both inorganic and organic pollutants, which are broadly reviewed by Bhattacharjee *et al.* (2020). Nowadays numerous researchers are trying to develop novel, low-cost, and ecologically viable adsorbents with high performance from waste products for the elimination of hazardous substances from wastewater. In the modern age, plastic products are extensively used in our daily activities. Polyethylene terephthalate (PET) is a widely used polymer around the world for its particular properties such as being lightweight, cost-effective, clearness, a good insulator, exceptional flexibility, and easy to handle (Djahed *et al.* 2016; Rahmawati *et al.* 2019), so a huge amount of plastic waste is generated yearly that is a pressing concern for the environment (El Essawy *et al.* 2017). PET is widely produced from public and industrial discarded materials that have no potential beneficiary application. Therefore, PET waste management is considered a global burden, especially in developing countries (Mallakpour & Behranvand 2016), where burning and landfilling are the commonly used disposal methods, which are highly responsible for environmental pollution by emitting toxic gaseous pollutants and polluting landfilling surrounding the ecosystem (e.g. aquatic and terrestrial) (Saha & Ghoshal 2005). Though recycling is another method for PET waste management instead of burning and landfilling, this method is not effective due to a lack of technical difficulties and lower economic return; in this viewpoint, activated carbon/char preparation (e.g. thermal and chemical activation) from PET waste would be a substitute technique as compared with other techniques (e.g. incineration, pyrolysis) (Djahed *et al.* 2016). Providentially, PET discarded products contain high carbon and lower impurities, which act as a new window for developing activated carbon/char and pollutants adsorbing agents (Cuerda-Correa *et al.* 2016). In experimental studies, process modeling and optimization are very important to improve the system performance, but conventional methods could optimize a single parameter at a time, which increases experimental time and cost (Gadekar & Ahammed 2019). Correct optimum conditions could not be attained because of the incompetence of experimental results to reflect relations among factors affecting the process (Musa *et al.* 2023). Recently, many researchers have paid attention to applying artificial neural networks (ANN) and response surface methodology (RSM) for optimizing and modeling the diverse experimental parameters at a time that enhances the system performance (Khan *et al.* 2020). Those machine learning approaches are a reliable and powerful tool that help overwhelm the system limitations and assess actual results using experimental data. Consequently, the combination of a smaller number of experiments and the hidden performances of post-process parameters could attain a more actual solution. So, modeling using the RSM and ANN approaches could assess the real associations between the input parameters and the response parameters of a process by applying experimental data (Gadekar & Ahammed 2019; Musa *et al.* 2023). It is a soft computing technique where required results can be achieved via alternating network weights (Gadekar & Ahammed 2019). So, it does not need any particular understanding of the physical/chemical procedure that moves the system. Nowadays, ANN- and RSM-based approaches have been used in diverse areas of environmental engineering, especially for water and wastewater treatment processes (Nair & Ahammed 2014; Agarwal *et al.* 2016; Karri & Sahu 2018; Musa *et al.* 2023), but very few studies have been conducted for HM adsorption. So, the objectives of this study were (i) to investigate the removal performance of carbonized PET plastic bottles for HM (Cd^{2+}, Pb^{2+}, Cu^{2+}, and Zn^{2+}) removal from simulated wastewater using diverse operational conditions such as pH, time of contact, HM concentration, and adsorbent dose applying machine learning statistical analysis; and (ii) to explore the adsorption mechanism using diverse models, such as isotherm, kinetic, and thermodynamic models.

2. MATERIALS AND METHODS

2.1. Materials and reagents

In the entire experiment, every chemical and reagent was laboratory-grade, purchased from Sigma-Aldrich (Germany), namely, $CuSO_4.5H_2O$ (≥98%), $ZnCl_2$ (≥98%), $PbCl_2$ (98%), and $CdCl_2$ (98%). The required amount of metal salts is used to prepare the stock solution (1,000 ppm), and the stock solution's pH value was less than 2.0 using HNO_3.

2.2. Adsorbent preparation from PET plastic bottle and characterization

Portable drinking water bottles were selected as PET plastic waste, collected from the local area, Jashore, Bangladesh. First, the waste bottle was washed with deionized water to remove visible impurities, cut into small sizes, and dried at 80 °C in an electric oven (Oven DSO-500D, Taiwan) until it was moisture free and cooled at ambient conditions. After that, char was produced by burning in an electric furnace at 600 °C for a 100 min retention time. Then, carbonized products were crushed, and preferred size portions (0.5–1.0 mm) were collected through a conventional sieve. Finally, they were stored in a sealed glass bottle for next experimental uses. The synthesized carbonized products were characterized using Fourier-transform infrared spectroscopy (FTIR) and scanning electron microscopy (SEM). The surface morphology of the prepared carbonized char was investigated with field emission scanning electron microscopy (FE-SEM) (Zeiss Sigma 300, Carl Zeiss, Germany) at 10 kV voltages. Before analysis, the carbonized powder was coated with gold for better imaging and to prevent native electrical charges. The surface chemistry was investigated by FTIR (Nicolet™ iS20, Thermo Scientific, USA), where the recorded spectra range varied from 400 to 4,000 cm^{-1} with 50 scans. The yield (%) of produced carbonized char was calculated using Equation (1):

$$\text{Yield (\%)} = \frac{\text{weight of the carbonized char in gram (g)}}{\text{weight of the used PET in gram (g)}} \times 100. \quad (1)$$

2.3. Adsorption experiments

The required quantity of metal salts was dissolved in distilled water to prepare 1,000 ppm stock solution and the retained stock solution's pH was less than 2.0 using HNO_3, and then successive dilution approaches were used to prepare the preferred working solution from the stock solution. The adsorption of HMs (Cd^{2+}, Pb^{2+}, Cu^{2+}, and Zn^{2+}) onto a carbonized adsorbent was carried out in a batch mode at 200 rpm using the following operational conditions: pH (3–7), time of contact (1–180 min), temperature (25–60 °C), adsorbent dose (0.5–6 g/L), and HMs (Cd^{2+}, Pb^{2+}, Cu^{2+}, and Zn^{2+}) concentration (25–300 mg/L). For pH adjustment, 0.1 N acid (HNO_3) and base (NaOH) solution were used. After a certain time, samples were taken, filtered, and acidified for metal analysis. Atomic absorption spectroscopy (AAS-7000, Shimadzu, Japan) was used to determine the concentration of HMs in raw and treated samples. A duplicate test was conducted to gather accurate results. The total HM adsorption rate and removal efficiency were estimated using Equations (2) and (3), respectively:

$$q_e = \frac{(C_0 - C_e)V}{m_s}, \quad (2)$$

$$R\ (\%) = \frac{(C_0 - C_e)}{C_0} \times 100, \quad (3)$$

where C_o is the initial HM concentration (mg/L), C_e is the equilibrium HM concentrations (mg/L), q_e is the amount of HMs adsorbed (mg/g), V is the volume of liquid solution (L), and m_s is the adsorbent mass (g).

2.4. Adsorption isotherm and kinetic experiments

Adsorption isotherm studies were carried out into 250 mL HM solutions of varied HM concentrations (25–300 mg/L), at pH 7, where 1 g/L carbonized char dose was added, and the solution was stirred at 200 rpm at 25 °C temperature for 90 min. While kinetic experiments were run in 300 mL HM solution at a fixed concentration (100 mg/L) and the other condition kept constant, then samples were taken out after the following time intervals 1, 5, 7, 10, 15, 20, 30, 60, 90, 120, 150, and 180 min; filtered; acidified; and analyzed. This study applied Langmuir and Freundlich isotherms for equilibrium data modeling, while pseudo-first-order and pseudo-second-order models were used for kinetic modeling (detailed in Table S1).

2.5. Error analysis

Error analysis is applied for every used model to assess the level of error as compared with obtained and experimental results. In this study, residual sum square (RSS), chi-square (χ^2) tests, and root mean square error (RMSE) error analysis test (Equations (4)–(6)) were calculated to determine which adsorption isotherm and kinetic models fitted to experimental data (Chakraborty *et al*. 2023a). A smaller error value denotes the model that fits the data the best. Equations (4)–(6) describe

the formula for determining the best-fit model:

$$\mathrm{RSS} = \sum (q_{\mathrm{exp}} - q_{\mathrm{cal}})^2, \tag{4}$$

$$\chi^2 = \sum \frac{(q_{\mathrm{exp}} - q_{\mathrm{cal}})^2}{q_{\mathrm{cal}}}, \tag{5}$$

$$\mathrm{RMSE} = \sqrt{\frac{\sum_{i=1}^{n} (q_{\mathrm{exp}} - q_{\mathrm{cal}})^2}{n}}, \tag{6}$$

where q_{exp} is the observed experimental adsorption data (mg/g) from the kinetic models, q_{cal} is the calculated adsorption data (mg/g) from models, and n represents the number of datasets.

2.6. Desorption study

For the desorption study, metal-loaded carbonized char was attained from adsorption isotherm experiments, filtered, and dried. Finally, the experiment was conducted in distilled water with diverse pH and stirring the solution at 200 rpm for 90 min. Equation (7) was applied to calculate the outcome:

$$\text{Desorption (\%)} = \frac{\text{Mass of metal ions desorbed (mg/L)}}{\text{Mass of metal ions adsorbed (mg/L)}} \times 100. \tag{7}$$

2.7. Adsorption thermodynamics

Thermodynamics is a vital parameter for adsorption study, where temperature variation is needed for conducting this study. In this study, Gibbs free energy change (ΔG), enthalpy (ΔH), and entropy (ΔS) are calculated by applying Equations (8)–(10):

$$K_d = \frac{q_e}{c_e}, \tag{8}$$

$$\Delta G = -RT \ln K_d, \tag{9}$$

$$\ln K_d = \frac{\Delta S}{R} - \frac{\Delta H}{RT}, \tag{10}$$

where T is the temperature (K), K_d is the equilibrium constant, and R is the universal gas constant (J mol^{-1} K^{-1}).

2.8. Process optimization

The Box–Behnken design (BBD) approach is an appropriate statistical tool widely used for process optimization, where the least number of experiments were applied to explore the probable association between the experimental parameters and their influences on the adsorbate adsorption (Gadekar & Ahammed 2019). This study uses a three-level three factorial BBD where three factors are defined as $X_1 =$ pH, $X_2 =$ metal concentration, and $X_3 =$ adsorbent dose, and three levels are stated as upper (1), central (0), and lower (−1) (detailed in Table S2). This model runs 17 experiments using Stat-Ease software (Design-Expert 13.0 trial version, Stat-Ease, Inc.). The following polynomial equation (Equation (11)) is used for BBD modeling:

$$Z = \beta_0 + \sum_{I=1}^{n} \beta_i A_i + \sum_{i=n}^{n} \beta_{ij} A_i A_j + \sum_{i=1}^{n} \beta_{ii} A_i^2, \tag{11}$$

where Z is the projected response (HM adsorption (%); q_e (Cd), q_e (Pb), q_e (Cu), q_e (Zn), $\beta_0 =$ Constant, $\beta_i =$ linear coefficient. $\beta_{ij} =$ interface coefficients, $\beta_{ii} =$ quadratic coefficients, and A_i and $A_j =$ process variables.

3. RESULTS AND DISCUSSION

3.1. Characterization of adsorbent

The yield of carbonized char was 18%, and Djahed *et al.* (2016) also recovered about 19% yield of carbonized PET plastic bottles. The point of zero charge (pzc) is the pH for which the net surface charge of the adsorbent is equal to zero (Lemessa *et al.* 2023). This study uses salt addition methods for pzc adopted from Mahmood *et al.* (2011). As illustrated in Figure 1(b), the plot of pH difference ((initial pH_i – final pH_f) vs initial (pH_i)) shows that pzc of carbonized char was obtained at pH = 2.99. According to the pzc concept, the adsorbent shows a positive attitude at solution pH < pzc value; conversely, a negative attitude is expressed at solution pH > pzc value. FTIR analysis represents the surface chemistry of the adsorbent (before and after adsorption), where diverse functional groups influence the linkage between the adsorbate and the adsorbent; results obtained are presented in Figure 1(a).

The adsorption peak near 1,600 cm^{-1} matching the in-plane C = C vibration indicates the graphite properties, which are the inborn properties of sp2 graphitic ingredients (Hu *et al.* 2017). The raw adsorbent shows four major peaks at 3,446, 2,930, 2,363, and 1,583 cm^{-1} (Figure S1a), indicating the stretching vibration of OH, C–H, C–N, and C = C, respectively (El Essawy *et al.* 2017). Slight alterations were observed after HM adsorption (Cd^{2+}, Pb^{2+}, Cu^{2+}, and Zn^{2+}) (Figure S1a); the above-mentioned adsorption peaks can link with the HM ions, while, more specifically, the hydroxyl group (OH^-) highly regulates the linkage between the adsorbent and the adsorbate. A similar result was reported by Chanda *et al.* (2021) for Ni adsorption using chemically treated mahogany sawdust. The surface feature of carbonized char (before and after adsorption) was estimated through SEM analysis; the results attained are presented in Figure S1. The EDX spectroscopy indicates that after the adsorption process, each HM is adsorbed onto the carbonized char surface (Figure S2b–e).

3.2. Adsorption behavior

3.2.1. Effect of contact time

To assess the adsorption behavior and equilibrium adsorption capabilities of carbonized adsorbent for HMs (Cd^{2+}, Pb^{2+}, Cu^{2+}, and Zn^{2+}), adsorption was evaluated at diverse contact times (presented in Figure 2(a)). These experiments were evaluated using a fixed metal concentration of 100 mg/L, temperature of 25 °C, pH equal to 7, and carbonized adsorbent mass of 1 g/L. Generally, three steps were involved during the adsorption process, as illustrated in Figure 2(a). Three stages controlled the whole adsorption procedure: (1) quick adsorption was achieved at an early stage (1–10 min) due to bulk concentration of HM ions and huge vacant space on the adsorbent surface; (2) after 10–90 min, the adsorption efficiency becomes slow due to the decline of existing binding sites with time; and (3) finally, the adsorption efficiency becomes comparatively very low within 90–180 min due to blocking of almost all vacant space (outer and inner site) on the adsorbent surface (Chakraborty *et al.* 2023b). So, adsorption reached equilibrium in 90 min, from all metals, which was chosen as the equilibrium contact

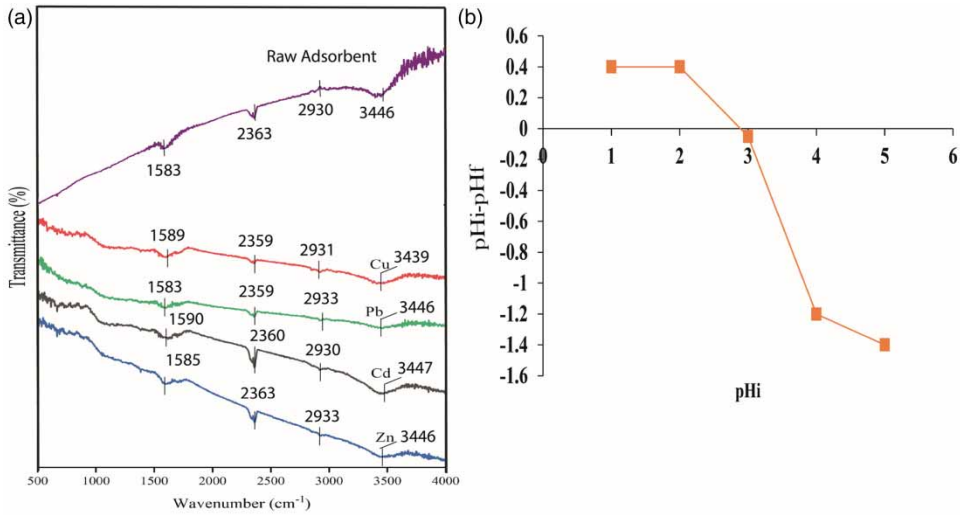

Figure 1 | (a) FTIR spectra of adsorbent and (b) pH of point zero charge.

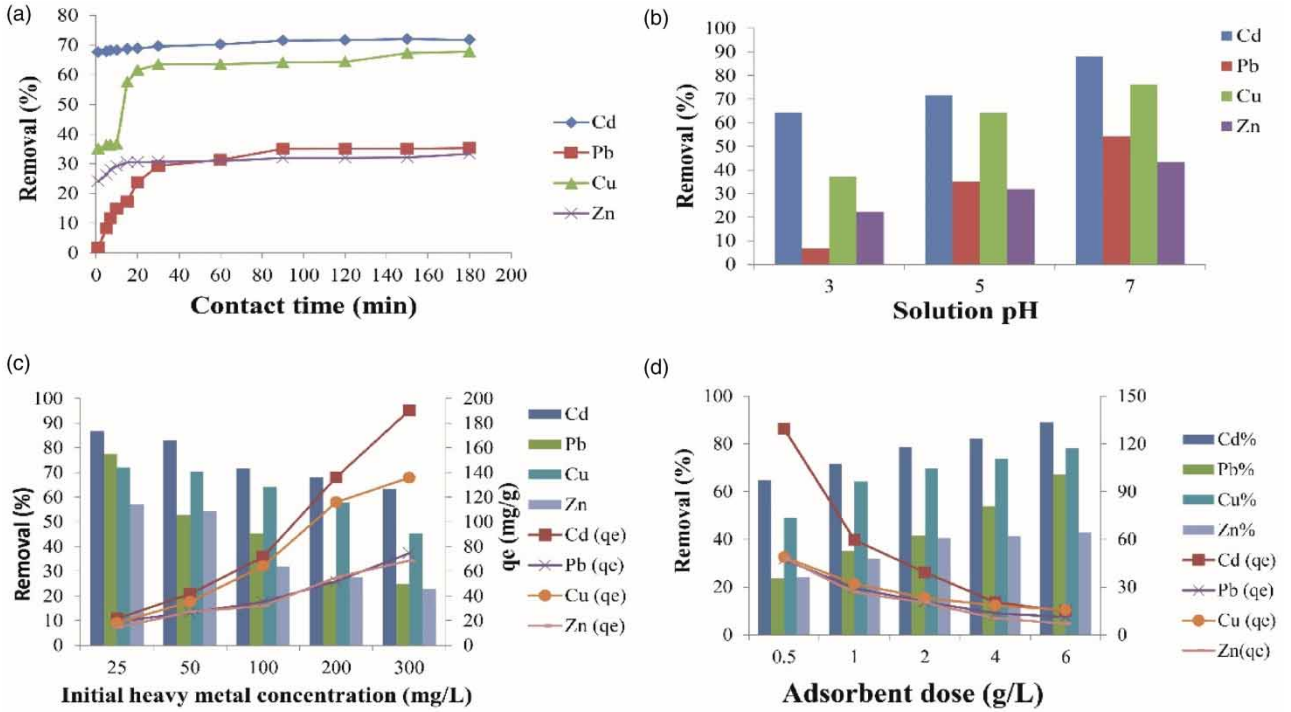

Figure 2 | Adsorption of HMs using carbonized char at diverse operational factors: (a) contact time, (b) pH, (c) initial HM concentration ((carbonized char dose = 1 g/L; HM concentration = 100 mg/L; optimum pH = 7), temperature = 25 °C; equilibrium contact time = 90 min)), and (d) adsorbent dose.

time for further experiments. Futalan *et al.* (2019) provide a similar explanation for the adsorption of HMs using spent coffee grounds.

3.2.2. Effect of pH

For adsorption science, pH is considered a vital factor because it influences the metal salt ionization rate, the modification of adsorbent inner and outer binding sites, and shifting of the adsorbent surface charge (Chakraborty *et al.* 2023a). Figure 2(b) shows the adsorption performance of HMs using carbonized adsorbent at varied solution pH of 3–7. The removal of HM increase (Cd^{2+} = 64–72%; Pb^{2+} = 7–35%; Cu^{2+} = 37–64% and Zn^{2+} = 22–32%) with increasing solution pH (3–7) (Figure 2(b)), because the surfaces of adsorbents were deprotonating, so electrostatic attraction between the absorbate and the adsorbent also increased at an increasing pH. The adsorbent surface becomes positive in a highly acidic environment due to the influence of oxygen-linked functional groups, where high proton clouds enrich electrostatic repulsion between adsorbate and adsorbent, resulting in lower HM removal. Though high pH increases the adsorption capacity, it also assists to precipitate the HMs by influencing the –OH group present in the solution confirmed by Wang & Qin (2005), which makes the adsorption study more complex. Therefore, a pH of 7 was selected as the optimum pH to avoid the precipitation of HMs. Similar results for the adsorption of HMs onto Carnauba straw powder were reported by Pereira *et al.* (2020).

3.2.3. Effect of initial HM concentration

To investigate the performance of carbonized adsorbents for HM adsorption with diverse concentrations (25–300 mg/L), an experiment was conducted where other factors were kept constant (t = 25 °C, contact time = 90 min, pH = 7, and dose = 1 g/L). Figure 2(c) shows that with increasing HM concentration (25–300 mg/L), the elimination performance of HMs (Cd^{2+} = 87–63%, Pb^{2+} = 77–25%, Cu^{2+} = 72–45%, and Zn^{2+} = 57–23%) (Figure 2(c)) decreases due to saturating carbonized adsorbent external surface at a fixed dose, where HM ions cover the vacant space. However, the adsorption capacity of the carbonized adsorbent increased (Cd^{2+} = 23–190 mg/g, Pb^{2+} = 19–74 mg/g, Cu^{2+} = 18–136 mg/g, and Zn^{2+} = 14–69 mg/g) due to a higher interface between HM ions and adsorbent active sites with increasing HM concentration, where high driving forces led to overcome the mass transfer between liquid and solid phases (Zaman *et al.* 2021).

3.2.4. Effect of adsorbent dose

Pollutant elimination from wastewater is significantly influenced by adsorbent dosage (Chakraborty *et al.* 2020). To assess the suitable adsorbent dose, batch adsorption experiments of HMs onto carbonized adsorbent were conducted at 25 ± 2 °C, with different adsorbent doses (1–6 g/L) and keeping the other conditions constant (pH = 7, HM concentration = 100 mg/L, CT = 90 min). Figure 2(d) reveals that the HM removal percentage improved with rising carbonized adsorbent doses (0.5–6 g/L) for HMs (Cd^{2+} = 64–89%, Pb^{2+} = 24–67%, Cu^{2+} = 49–78%, and Zn^{2+} = 24–43%), respectively, due to lots of active exchangeable sites on the carbonized adsorbent surface, resulting in greater adsorption (Chakraborty *et al.* 2023a). While the adsorption capacity gradually reduces (Cd^{2+} = 129–15 mg/g, Pb^{2+} = 47–11 mg/g, Cu^{2+} = 49–15 mg/g, and Zn^{2+} = 48–7 mg/g) with increasing adsorption dose (0.5–6 g/L) might be the aggregation of HM ions onto the carbonized adsorbent. A related elucidation was given by Al-Malack & Basaleh (2016).

3.3. Kinetic models and adsorption mechanism

Adsorption kinetics is needed to design an effluent treatment plant unit, where the adsorbent could remove pollutants at a certain rate. In the present study, two commonly used kinetics models such as Lagergren's pseudo-first-order and Ho's pseudo-second-order, were applied for HM (Cd^{2+}, Pb^{2+}, Cu^{2+}, and Zn^{2+}) adsorption onto carbonized adsorbents. The model accuracy depends on the high correlation coefficient (R^2) and lower error values (RSS, chi-square (χ^2), and RMSE) of the model, and the applied model parameters are shown in Table 1. The pseudo-second-order kinetic model shows higher R^2 and lower RSS, χ^2, and RMSE values for HM adsorption as compared with pseudo-first-order kinetic; in addition, the calculated ($q_{e,\mathrm{cal}}$) value from the pseudo-second-order kinetic model also corresponds to the experimental value ($q_{e,\mathrm{exp}}$), indicating that pseudo-second-order was the best-fitted kinetic model for adsorption data. Therefore, chemical adsorption controlled the total adsorption process (i.e. electrostatic interactions between the absorbate and adsorbent), where rapid adsorption occurred at the first phase and gradually slowed at time progress due to the lack of adsorbent site that is supported by Figure 2(a); previous studies also reported a similar outcome (Chakraborty *et al.* 2023d; Lemessa *et al.* 2023).

The experimental data were also evaluated by intraparticle (IP) diffusion to determine the diffusion mechanisms. The IP plot did not pass through the origin (Figure S3) and high intercept values (Table 2), representing that exterior diffusion was the rate-limiting step as interior diffusion for HM adsorption using carbonized adsorbent, which may happen at the same time. Futalan *et al.* (2019), Chanda *et al.* (2021), and Chen *et al.* (2022) observed related findings in their adsorption study.

Table 1 | Kinetic parameters for HMs adsorption onto carbonized char

Models	Parameters	Cd^{2+}	Cu^{2+}	Pb^{2+}	Zn^{2+}
	$q_{e,\mathrm{exp}}$ (mg/g)	70.470	64.120	35.040	31.930
Pseudo-first-order	$q_{e,\mathrm{cal}}$ (mg/g)	3.291	28.635	29.362	4.348
	K_1 (min^{-1})	0.041	0.078	0.038	0.0317
	R^2	0.993	0.774	0.911	0.631
	RSS	54,845.950	13,976.130	403.754	9,076.489
	χ^2	2,239.826	55.764	1.885	301.835
	RMSE	67.605	34.127	5.800	27.502
Pseudo-second-order	$q_{e,\mathrm{cal}}$ (mg/g)	71.942	68.493	39.215	32.894
	K_2 (g/mg/min)	0.021	0.003	0.001	0.017
	H (mg/g/min)	112.35	15.673	2.423	19.267
	R^2	1.000	0.998	0.996	0.999
	RSS	81.569	227.062	27.279	154.603
	χ^2	0.099	0.343	0.099	0.449
	RMSE	2.607	4.349	1.507	3.589
IP diffusion	K_{diff} ($\mathrm{mg/g/min}^{0.5}$)	0.386	2.690	2.596	0.536
	C (mg/g)	67.159	37.302	6.641	26.548
	R^2	0.966	0.678	0.735	0.833

3.4. Adsorption isotherm modeling

The link between an adsorbate and an adsorbent in an adsorption study is well explained by adsorption isotherms. In this present study, Langmuir and Freundlich isotherms were used, which are usually beneficial in the solid/liquid system, presented in Table 2. Langmuir isotherm was the best-fitted isotherm for Cu^{2+} adsorption onto a carbonized adsorbent due to its higher correlation coefficient value ($R^2 = 0.972$), lower error (RSS = 0.689), chi-square value ($\chi^2 = 0.044$), and RMSE (0.262) as compared to the Freundlich isotherm ($R^2 = 0.937$, RSS = 4.610; RSME = 0.679, and $\chi^2 = 0.313$) (Table 1), revealing that Cu^{2+} molecules produce a single continuous layer with similar dispersal to carbonized char, while Cd^{2+}, Pb^{2+}, and Zn^{2+} follow the Freundlich isotherm than Langmuir concerning correlation coefficients and error values, showing multi-layer adsorption onto carbonized adsorbents.

The monolayer maximum adsorption capacity of HMs onto carbonized adsorbent was 263.157, 78.740, 196.078, and 84.745 mg/g for Cd^{2+}, Pb^{2+}, Cu^{2+}, and Zn^{2+}, respectively (Table 2). The R_L values of carbonized char were between 0 and 1, representing that HM adsorption onto carbonized adsorbents was appropriate under the studied experimental conditions. Conversely, the value of adsorption intensity (n) was higher than 1, and higher K_F demonstrated that the adsorption process was promising for HM adsorption from aqueous solutions using carbonized adsorbents (Table 2). This study outcome is also in correspondence with the findings of El Essawy *et al.* (2017). In addition, the performance of HM adsorption using carbonized adsorbents is comparable with other adsorbents, as presented in Table S3.

3.5. Adsorption thermodynamics studies

A thermodynamic study represents the role of temperature in adsorption, the nature of the linkage between the adsorbate and the adsorbent, and the direction and mechanism of reaction with changing the experimental temperature (Chakraborty *et al.* 2023d). These study results are presented in Table S4 and Figure S5a. A Van't Hoff plot of ln K_d vs $1/T$ made a straight line (not shown in the figure) with R^2 values of 0.798, 0.996, 0.931, and 0.954 for Cd^{2+}, Pb^{2+}, Cu^{2+}, and Zn^{2+}, respectively. Table S4 shows that negative values of ΔG^0 demonstrate that HM adsorption processes are thermodynamically spontaneous and useful (El Essawy *et al.* 2017). The exothermic type of adsorption is confirmed by the negative result of ΔH^0, HM ion adsorption decreases with rising temperature, and no remarkable deviations were found after 298 K (250 °C). Therefore, the next experiments were conducted at this temperature. The positive ΔS^0 also suggests the decreasing chance between the carbonized adsorbent and metal ion interface, which mainly occurred through the chemical adsorption mechanism through the ion exchange process. Sahmoune (2019) detected the exothermic reaction for HM adsorption using green adsorbents.

3.6. BBD and regression model

For process optimization, the three factors including pH, initial HMs concentration, and the adsorbent dose were applied, and the studied responses are presented in Table S5 and Figures 3 and 4, respectively. The elimination of HMs ranges from 63.4 to 86.68%, 13.78 to 67.1%, 37 to 73.66%, and 2.22 to 57.04% for Cd^{2+}, Pb^{2+}, Cu^{2+}, and Zn^{2+}, respectively

Table 2 | Isotherm parameters for adsorption of HMs onto carbonized char

Isotherm models	Parameters	Cd^{2+}	Cu^{2+}	Pb^{2+}	Zn^{2+}
Langmuir	q_{max} (mg/g)	263.157	196.078	78.740	84.745
	b (L/mg)	0.019	0.0147	0.025	0.014
	R_L	0.148–0.677	0.184–0.730	0.115–0.610	0.187–0.734
	R^2	0.884	0.991	0.927	0.923
	RSS	728.385	76.321	265.284	385.644
	χ^2	1.556	0.207	1.235	1.711
	RMSE	12.069	3.906	7.284	8.782
Freundlich	K_F (mg/g) (L/mg)$^{1/n}$	10.480	5.722	9.819	5.033
	n	1.639	1.535	2.805	2.104
	R^2	0.992	0.9773	0.952	0.953
	RSS	150.350	732.773	124.494	241.169
	χ^2	0.328	1.963	0.577	1.080
	RMSE	5.483	12.105	4.989	6.945

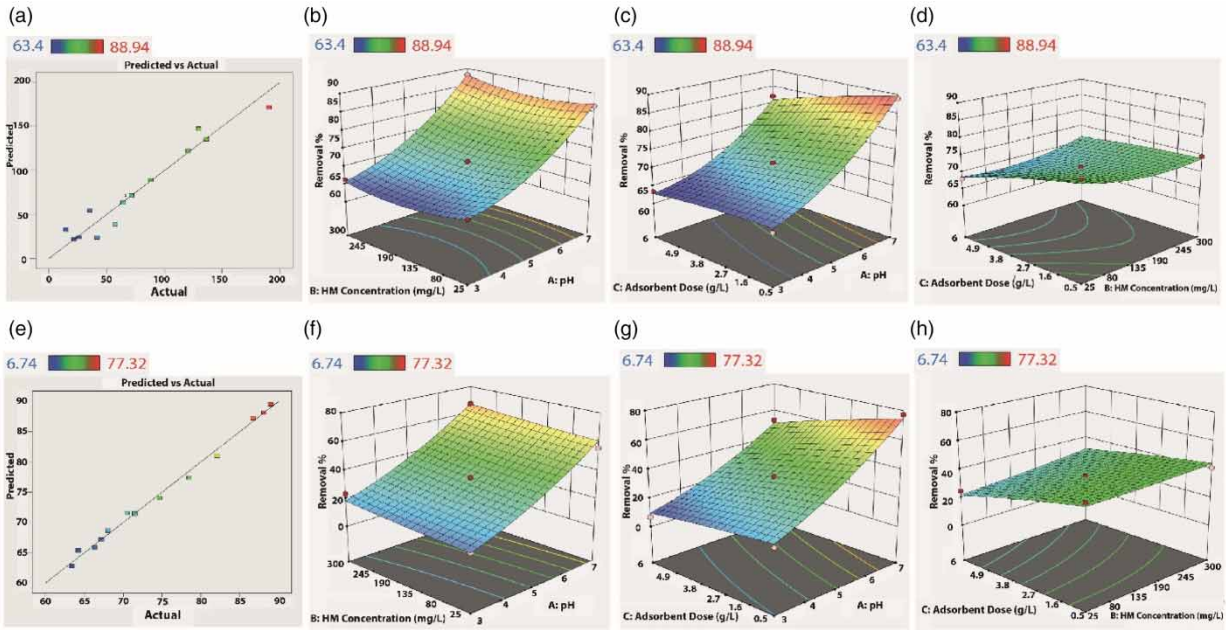

Figure 3 | BBD for Cd^{2+} ((a) actual vs predicted plot, (b) pH, (c) adsorbent dose, and (d) initial concentration) and Pb^{2+} ((e) actual vs predicted plot, (f) pH, (g) adsorbent dose, and (h) initial HM concentration); color spectra show highest (red) to lowest (blue) removal efficiency.

(Table S5). The BBD produces 3D surface plots to understand the relation between the tested variables. This design also helps identify the ideal experimental settings (Kousha *et al.* 2015). Figures 3 and 4 show the effect of solution pH, initial HM concentration, and adsorbent dose on HM elimination efficiency using prepared carbonized adsorbent. Due to increasing solution pH, the interaction between positive charge adsorbate and negatively charged adsorbent increased; consequently, the maximum removal was achieved at a pH of 7. A high carbonized adsorbent dose provides greater surface areas and

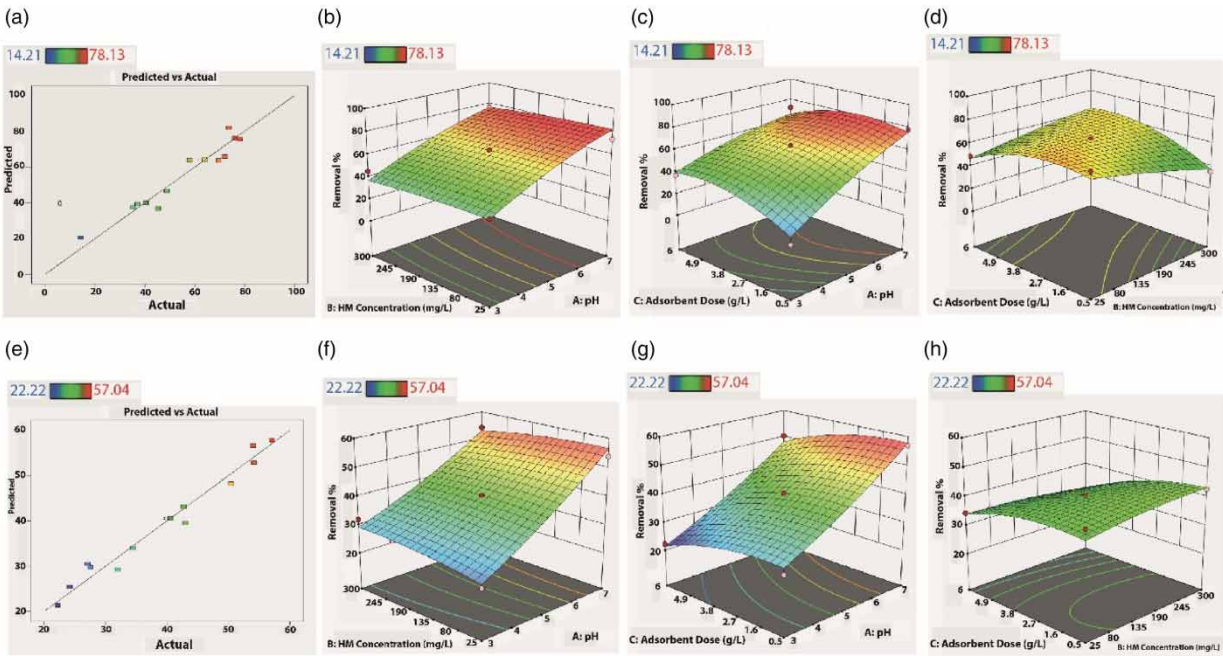

Figure 4 | BBD for Cu^{2+} ((a) actual vs predicted plot, (b) pH, (c) adsorbent dose, and (d) initial concentration) and Zn^{2+} ((e) actual vs predicted plot, (f) pH, (g) adsorbent dose, and (h) initial HM concentration); color spectra shows highest (red) to lowest (blue) removal efficiency.

huge exchangeable sites, resulting in greater adsorption performance achieved at the maximum adsorbent dose. The HM removal efficiency decreased with increasing HM concentration from 25 to 300 mg/L, and the highest removal was found at 25 mg/L for all HMs.

The statistical association between the nominated experimental factors and the response was explained by a quadratic model with corresponding coded factors and are best fitted using the following equations:

$$\textbf{Removal (Cu\%)} = 64.12200 + 20.38625X_1 - 2.25625X_2 + 2.32750X_3 - 0.642500X_1 \times X_2 - 7.20000X_1 \times X_3 + 10.87500X_2 \times X_3 - 3.93475X_1^2 - 1.36975X_2^2 - 9.82225X_3^2, \quad (12)$$

$$\textbf{Removal (Zn\%)} = 40.55800 + 13.71500X_1 + 0.043750X_2 - 4.52375X_3 - 1.90750X_1 \times X_2 - 0.337500X_1 \times X_3 - 1.76500X_2 \times X_3 + 1.49100X_1^2 - 1.00650X_2^2 - 2.75650X_3^2, \quad (13)$$

$$\textbf{Removal (Cd\%)} = 71.46000 + 10.58000X_1 - 0.095000X_2 - 2.78500X_3 + 0.565000X_1 \times X_2 - 1.50500X_1 \times X_3 + 1.56000X_2 \times X_3 + 3.68000X_1^2 + 1.93500X_2^2 - 0.475000X_3^2, \quad (14)$$

$$\textbf{Removal (Pd\%)} = 35.15400 + 23.87625X_1 + 2.69250X_2 - 8.56875X_3 + 0.367500X_1 \times X_2 - 3.32500X_1 \times X_3 + 1.91750X_2 \times X_3 + 4.25550X_1^2 + 0.663000X_2^2 - 0.704500X_3^2. \quad (15)$$

Analysis of variance (ANOVA) is an analytical technique that is applied to detect the validity and suitability of Fisher's, *F*-test, and Student's *t*-test models. The input effective variables (A = pH, B = HMs concentration, and C = adsorbent dose) were considered for statistical evaluation of the empirical models, presented in Tables S6–S9, respectively, where pH (A) and adsorbent dose (C) show a significant effect for HM removal from aqueous solution. The *p*-values of all quadratic models ($Cd^{2+} = 0.0001$, $Pb^{2+} = 0.0001$, $Cu^{2+} = 0.0020$, and $Zn^{2+} = 0.0002$) were less than 0.05, suggesting that the quadratic model fits the HM (Cd^{2+}, Pb^{2+}, Cu^{2+}, and Zn^{2+}) adsorption data on the carbonized adsorbent. Lack of fit is more significant than the pure error in terms of the *p*-value ($p < 0.0001$), revealing that the design model precisely explains the data performance for the experiments and the factors examined have very significant effects on removal efficiency (Chakraborty *et al.* 2023d). In addition, A (pH), C (adsorbent dose), AC (pH–adsorbent dose), BC (HM concentration–adsorbent dose), A^2 (pH), and B^2 (HM concentration) are significant model ($p < 0.05$) terms for HM adsorption using carbonized adsorbents. Moreover, the R^2 value of the HM adsorption quadratic model ($Cd^{2+} = 0.99$, $Pb^{2+} = 0.97$, $Cu^{2+} = 0.94$, and $Zn^{2+} = 0.98$) showed that 99, 97, 94, and 98% of the whole variability of the result was explained by this model. A good agreement was attained between experimental (R^2) and projected (R^2adj) results for all HMs (Figures 3 and 4), showing that the model is a good fit, where most of the data point near the straight line. On the other hand, the *F*-values of Cd^{2+}, Pb^{2+}, Cu^{2+}, and Zn^{2+} were 118.05, 39.47, 11.42, and, 25.50, respectively, suggesting that the models are significant. There is only a 0.01, 0.01, 0.20, and 0.02% chance of creating noise for Cd^{2+}, Pb^{2+}, Cu^{2+}, and Zn^{2+} adsorption onto carbonized adsorbent due to higher *F*-value, respectively. The signal-to-noise ratio for Cd^{2+} (34.99), Pb^{2+} (21.81), Cu^{2+} (12.01), and Zn^{2+} (17.26) was larger than 4 representing a satisfactory signal. So, these quadratic models are suitable for explaining the adsorption of HMs onto CPETPW. Renu *et al.* (2018) and Rouniasi *et al.* (2018) used this model for HM adsorption from wastewater using activated carbon oxide nanosheets and modified wheat bran, respectively.

3.7. ANN modeling

ANNs are widely used for recording the non-linear relation between independent and dependent variables and are suitable to apply to any condition (Gadekar & Ahammed 2019). This study applies a multi-level feed-forward neural network, which is directed in the following order: input–hidden–output. The applied ANN has 60% training, 20% validation, and 20% testing networks. The input parameters (pH, adsorbent dose, and initial HM concentration) were selected for ANN, while the percentage of HM removal was selected as the output layer. Trial and error techniques were applied to achieve model accuracy, and validation and testing were carried out using MATLAB (R2020a).

Figure 5 represents the topology for HMs adsorption including 3:5:1, 3:4:1, 3:4:1 and 3:5:1 for Cd^{2+}, Pb^{2+}, Cu^{2+}, and Zn^{2+}, respectively (Table S10). The high and low frequencies of hidden neurons directly affect the ANN presentation and the appraisal of accuracy. So, the ideal quantities of hidden neuron selection assist in escaping over- and under-estimation (Gadekar & Ahammed 2019). ANN performance is improved with rising neuron numbers, but the coefficients of the

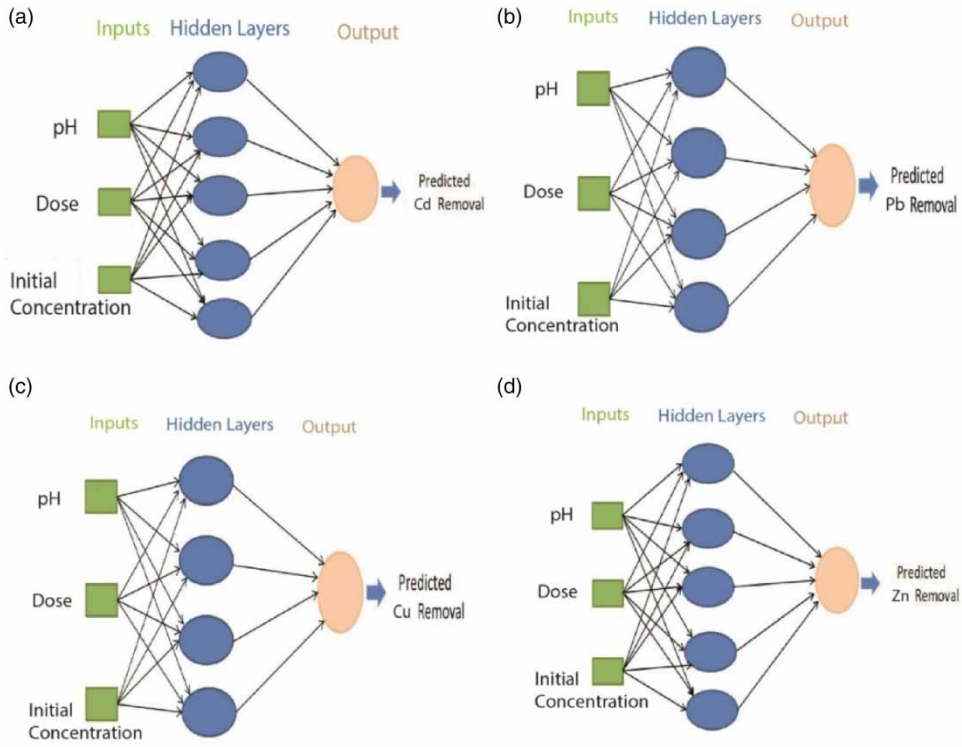

Figure 5 | ANN network with topology: (a) Cd^{2+}, (b) Pb^{2+}, (c) Cu^{2+}, and (d) Zn^{2+}.

determinant (R^2) did not represent the same outcome in the training phase. In the case of all HM (Cd^{2+}, Pb^{2+}, Cu^{2+}, and Zn^{2+}) adsorption, all training, validation, and testing phases of tan-sigmoidal and topology were selected according to a high *R*-value and its associated lower MSE value (Table S10). Good associations between experimental and ANN-predicated results (Figures 6 and 7) indicate that the ANN model was suitable for describing HM adsorption using carbonized char. Khajeh *et al.* (2012) and Khan *et al.* (2020) stated the same relevant result for HM adsorption modeling using ANN.

3.8. Real wastewater experiment

This study utilizes carbonized adsorbents for exploring the performance of removing HMs from real wastewater (RWW) experiments, where wastewater collected from an industrial area and optimum experiment conditions (adsorbent dose = 1 g/L, optimum pH = 7, temperature = 25 °C, and equilibrium contact time = 90 min) were applied for capitalizing the performance of the adsorbent in RWW. The properties of the collected wastewater were as follows: pH = 5.2, conductivity = 8,840 μS/cm, and total dissolved solids = 4,231 mg/L. The initial concentration of Cd^{2+}, Pb^{2+}, Cu^{2+}, and Zn^{2+} in RWW was 0.501, 19.260, 0.683, and 0.355 mg/L, respectively. After the treatment at pH 7, the concentration was 0.004, 7.280, 0.012, and 0.126 mg/L, respectively. The removal rates of HMs (Cd^{2+}, Pb^{2+}, Cu^{2+}, and Zn^{2+}) were 99.2, 62.2, 97.6, and 64.4%, respectively (Figure S4), suggesting that a carbonized adsorbent will be suitable for eliminating HMs (Cd^{2+}, Pb^{2+}, Cu^{2+}, and Zn^{2+}) from industrial wastewater.

3.9. Desorption study

This process is applied to assess the possibility of further contamination when the treated adsorbent comes into the environment. The desorption rate of the adsorbent is significantly influenced by the nature of bonding (ionic bonds, Van der Waals forces, or covalent) between adsorbate and adsorbent (Chakraborty *et al*. 2023a). Here, a desorption study was conducted with diverse pH values (pH 5–11), where carbonized chars were taken from isotherm studies, dried, and the required amount was used for experiments. Figure S5b shows that the desorption percentage of HMs (Cd^{2+}, Pb^{2+}, Cu^{2+}, and Zn^{2+}) was not increasing significantly instead of increasing pH, which might be the possibility of the existing strong chemical

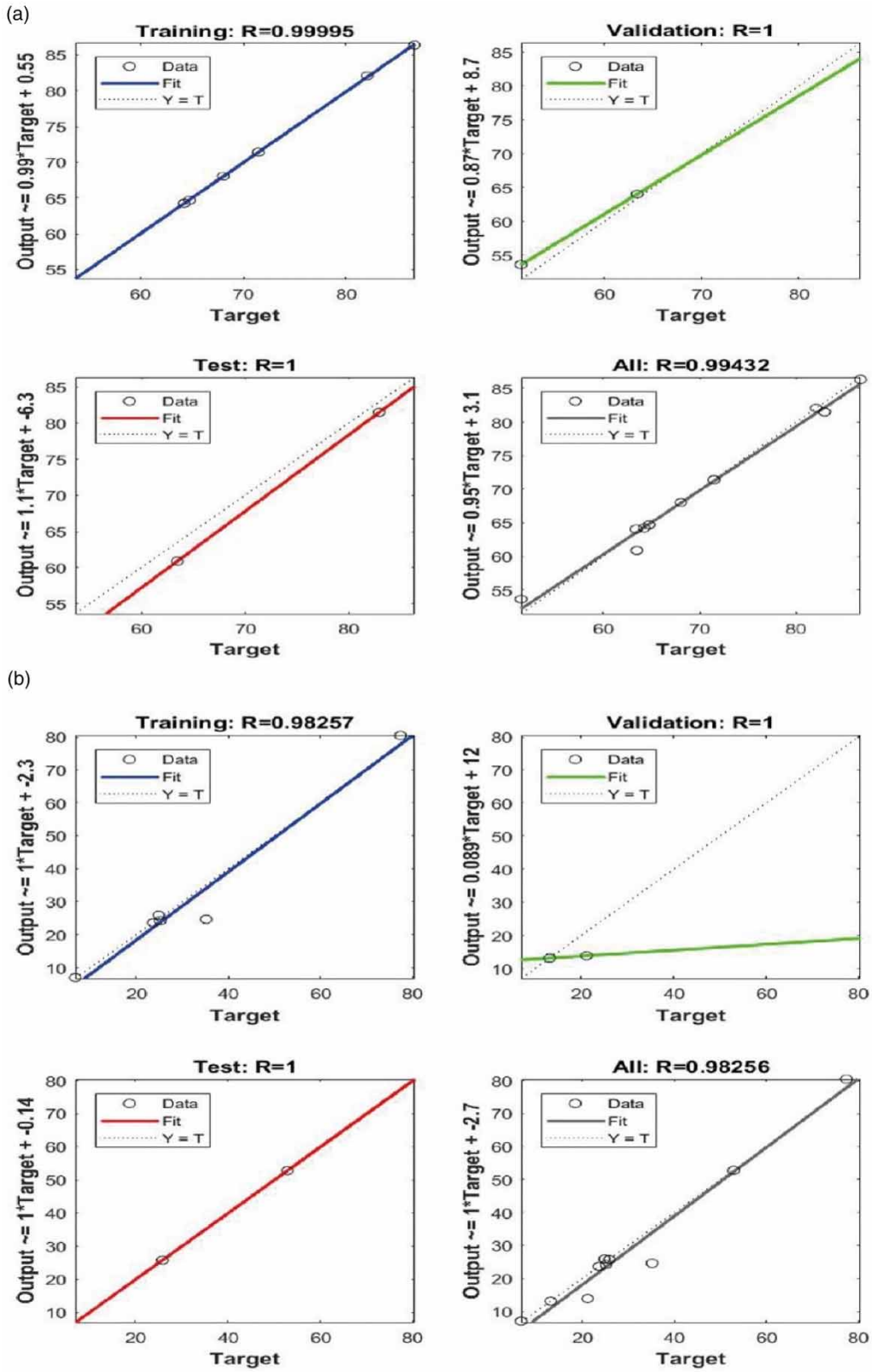

Figure 6 | Linear fit for experimental and predicted concentration removal using ANN for (a) Cd^{2+} and (b) Pb^{2+}.

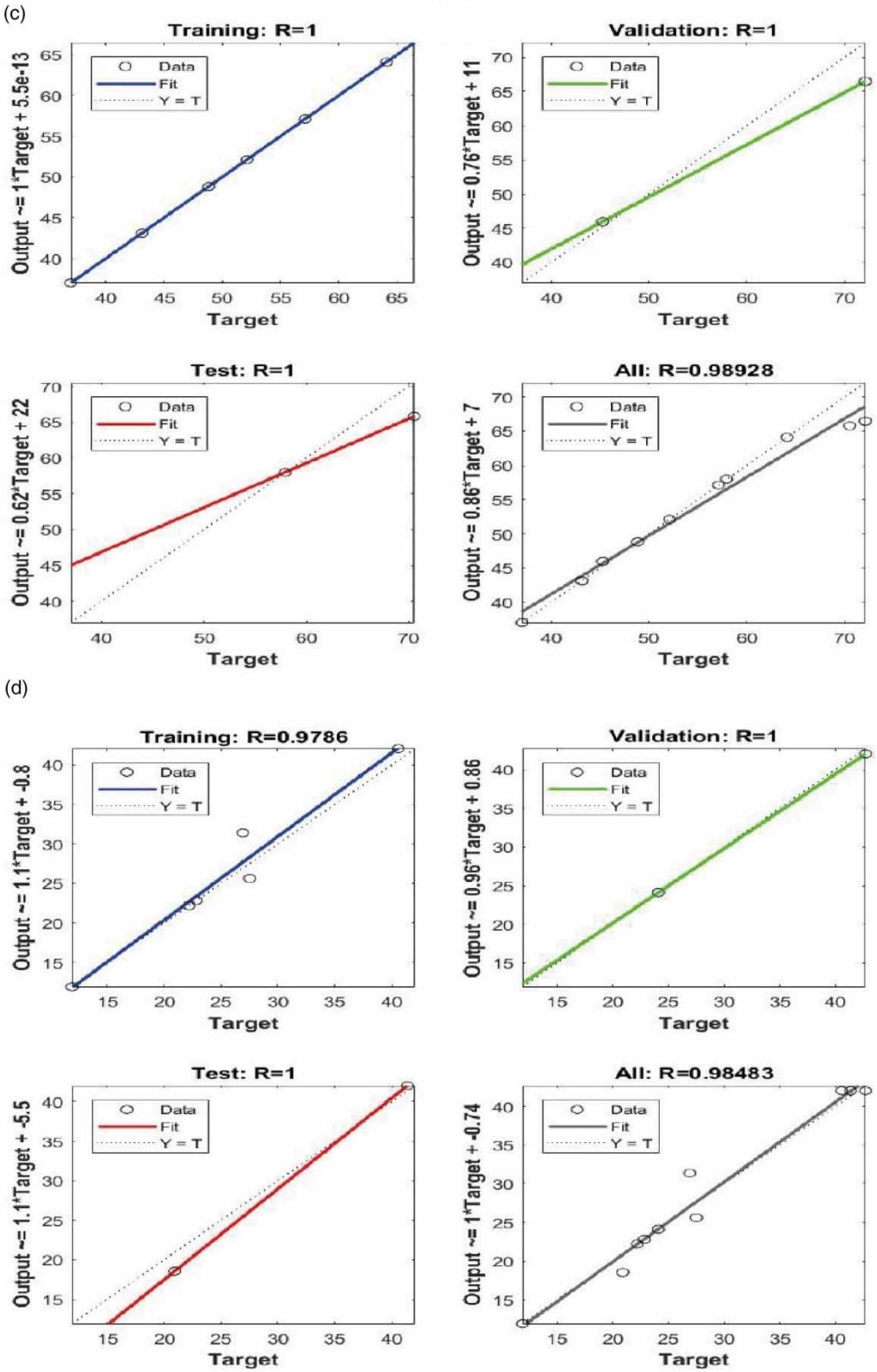

Figure 7 | Linear fit for experimental and predicted concentration removal using ANN for (c) Cu^{2+} and (d) Zn^{2+}.

bonding between HM ions and carbonized adsorbent (Figure S7), confirming the eco-friendly properties. Mouni *et al.* (2018) and Chakraborty *et al.* (2021b) provide a similar explanation in their study.

4. CONCLUSIONS

The presence of HMs in the environment from industrial sources is a matter of great concern. So, this study tried to develop a new, inexpensive, and environmentally friendly wastewater treatment method where carbonized char is produced from PET bottle waste for removing HMs from wastewater. The study finding shows that carbonized adsorbent shows high performance in removing HMs from wastewater. The elimination efficiency of HMs decreases with increasing HMs concentration and temperature while enhancing with increasing adsorbent dose. The equilibrium contact time of all HMs was 90 min. BBD and ANN models showed a good agreement between the predicted and experimental results. Pseudo-second-order was the best-matching kinetic model for HM adsorption data. The equilibrium data were well explained by the Langmuir isotherm for Cu^{2+}, while the Freundlich isotherm was used for Cd^{2+}, Pb^{2+}, and Zn^{2+}. Thermodynamic study shows that the adsorption is exothermic and spontaneous for HM removal. According to the study performance, carbonized char could be a suitable and effective adsorbent for removing HMs (Cd^{2+}, Pb^{2+}, Cu^{2+}, and Zn^{2+}) from wastewater, where a centralized wastewater treatment system is not accessible.

ACKNOWLEDGEMENTS

The authors would like to thank the Department of Environmental Science and Technology, Jashore University of Science and Technology, Jashore 7408, Bangladesh, for providing access to laboratory facilities.

DATA AVAILABILITY STATEMENT

All relevant data are included in the paper or its Supplementary Information.

CONFLICT OF INTEREST

The authors declare there is no conflict.

REFERENCES

Agarwal, S., Tyagi, I., Gupta, V. K., Bagheri, A. R., Ghaedi, M., Asfaram, A. & Bazrafshan, A. A. 2016 Rapid adsorption of ternary dye pollutants onto copper (I) oxide nanoparticle loaded on activated carbon: Experimental optimization via response surface methodology. *Journal of Environmental Chemical Engineering* **4** (2), 1769–1779. https://doi.org/10.1016/j.jece.2016.03.002.

Al-Malack, M. H. & Basaleh, A. A. 2016 Adsorption of heavy metals using activated carbon produced from municipal organic solid waste. *Desalination and Water Treatment* **57** (51), 24519–24531. https://doi.org/10.1080/19443994.2016.1144536.

Barakat, M. A. 2011 New trends in removing heavy metals from industrial wastewater. *Arabian Journal of Chemistry* **4** (4), 361–377. https://doi.org/10.1016/j.arabjc.2010.07.019.

Bhattacharjee, C., Dutta, S. & Saxena, V. K. 2020 A review on biosorptive removal of dyes and heavy metals from wastewater using watermelon rind as biosorbent. *Environmental Advances* **2**, 100007. https://doi.org/10.1016/j.envadv.2020.100007.

Boulaiche, W., Hamdi, B. & Trari, M. 2019 Removal of heavy metals by chitin: Equilibrium, kinetic and thermodynamic studies. *Applied Water Science* **9**, 1–10. https://doi.org/ 10.1007/s13201-019-0926-8.

Chakraborty, T. K., Islam, M. S., Zaman, S., Kabir, A. H. M. E. & Ghosh, G. C. 2020 Jute (*Corchorus olitorius*) stick charcoal as a low-cost adsorbent for the removal of methylene blue dye from aqueous solution. *SN Applied Science* **2** (4), 765.

Chakraborty, T. K., Hossain, M. R., Ghosh, G. C., Ghosh, P., Sadik, A., Habib, A. & Rahman, M. M. 2021a Distribution, source identification and potential ecological risk of heavy metals in surface sediments of the Mongla port area, Bangladesh. *Toxin Reviews* **41** (3), 834–845. https://doi.org/10.1080/15569543.2021.1942065.

Chakraborty, T. K., Ghosh, G. C., Akter, M., Adhikary, K., Islam, M., Ghosh, P. & Kabir, A. H. M. 2021b Biosorption of reactive red 120 Dye from aqueous solutions by using mahagoni *(Swietenia mahagoni)* wood and bark charcoal: Equilibrium, and kinetic studies. *Pollution* **7** (4), 905–921. https://doi.org/10.22059/poll.2021.325135.1110.

Chakraborty, T. K., Ghosh, G. C., Hossain, M. R., Islam, M. S., Habib, A., Zaman, S. & Khan, A. S. 2022a Human health risk and receptor model-oriented sources of heavy metal pollution in commonly consume vegetable and fish species of high Ganges River floodplain agro-ecological area, Bangladesh. *Heliyon* **8** (10), e11172. https://doi.org/10.1016/j.heliyon.2022.e11172.

Chakraborty, T. K., Islam, M. S., Ghosh, G. C., Ghosh, P., Zaman, S., Habib, A. & Josy, M. S. K. 2022b Human health risk and hydro-geochemical appraisal of groundwater in the southwest part of Bangladesh using GIS, water quality indices, and multivariate statistical approaches. *Toxin Reviews* 1–15. https://doi.org/10.1080/15569543.2022.2134572.

Chakraborty, T. K., Audhikary, K., Ghosh, G. C., Rahman, M. S., Habib, A., Islam, M. S. & Hossain, N. 2023a Adsorption of acid and basic dye from the simulated wastewater using carbonized microplastic particles synthesized from recycled polyethylene terephthalate plastic waste bottles: An integrated approach for experimental and practical applications. *AQUA – Water Infrastructure, Ecosystems and Society* **72** (4), 491–506.

Chakraborty, T. K., Ghosh, S., Islam, M. S., Nice, M. S., Islam, K. R., Netema, B. N. & Halder, M. 2023b Removal of hazardous textile dye from simulated wastewater by municipal organic solid waste charcoal using machine learning approaches: Kinetics, isotherm, and thermodynamics. *Heliyon* **9**, 8.

Chakraborty, T. K., Tammim, L., Islam, K. R., Nice, M. S., Netema, B. N., Rahman, M. S. & Rahman, M. A. 2023c Black carbon derived PET plastic bottle waste and rice straw for sorption of Acid Red 27 dye: Machine learning approaches, kinetics, isotherm and thermodynamic studies. *PLoS One* **18** (8), e0290471.

Chakraborty, T. K., Islam, M. S., Ghosh, G. C., Ghosh, P., Zaman, S., Hossain, M. R. & Khan, A. S. 2023d Receptor model-based sources and risks appraisal of potentially toxic elements in the urban soils of Bangladesh. *Toxicology Reports* **10**, 308–319. https://doi.org/10.1016/j.toxrep.2023.02.011.

Chanda, R., Mithun, A. H., Hasan, M. A. & Biswas, B. K. 2021 Nickel removal from aqueous solution using chemically treated mahogany sawdust as biosorbent. *Journal of Chemistry* 1–10. https://doi.org/10.1155/2021/4558271.

Chen, W. S., Chen, Y. C. & Lee, C. H. 2022 Modified activated carbon for copper ion removal from aqueous solution. *Processes* **10** (1), 150. https://doi.org/10.3390/pr10010150.

Cuerda-Correa, E. M., Alexandre-Franco, M. F., Fernßndez-Gonzßlez, C. & Gómez-Serrano, V. 2016 Preparation of high-quality activated carbon from polyethyleneterephthalate (PET) bottle waste. Its use in the removal of pollutants in aqueous solution. *Journal of Environmental Management* **181**, 522–535. https://doi.org/10.1016/j.jenvman.2016.06.070.

Djahed, B., Shahsavani, E., Khalili Naji, F. & Mahvi, A. H. 2016 A novel and inexpensive method for producing activated carbon from waste polyethylene terephthalate bottles and using it to remove methylene blue dye from aqueous solution. *Desalination and Water Treatment* **57** (21), 9871–9880. https://doi.org/10.1080/19443994.2015.1033647.

El Essawy, N. A., Ali, S. M., Farag, H. A., Konsowa, A. H., Elnouby, M. & Hamad, H. A. 2017 Green synthesis of activated carbon from recycled PET bottle wastes for use in the adsorption of dyes in aqueous solution. *Ecotoxicology and Environmental Safety* **145**, 57–68. https://doi.org/10.1016/j.ecoenv.2017.07.014.

Futalan, C. M., Kim, J. & Yee, J. J. 2019 Adsorptive treatment via simultaneous removal of copper, lead and zinc from soil washing wastewater using spent coffee grounds. *Water Science & Technology* **79** (6), 1029–1041. https://doi.org/10.2166/wst.2019.087.

Gadekar, M. R. & Ahammed, M. M. 2019 Modelling dye removal by adsorption onto water treatment residuals using combined response surface methodology-artificial neural network approach. *Journal of Environmental Management* **231**, 241–248. https://doi.org/10.1016/j.jenvman.2018.10.017.

Ghosh, G. C., Samina, Z. & Chakraborty, T. K. 2018 Adsorptive removal of Cr (VI) from aqueous solution using rice husk and rice husk ash. *Desalination and Water Treatment* **130**, 151–160. http://dx.doi.org/10.5004/dwt.2018.22828.

Ghosh, G. C., Khan, M. J. H., Chakraborty, T. K., Zaman, S., Kabir, A. E. & Tanaka, H. 2020a Human health risk assessment of elevated and variable iron and manganese intake with arsenic-safe groundwater in Jashore, Bangladesh. *Scientific Reports* **10** (1), 5206. https://doi.org/10.1038/s41598-020-62187-5.

Ghosh, G. C., Chakraborty, T. K., Zaman, S., Nahar, M. N. & Kabir, A. H. M. E. 2020b Removal of methyl orange dye from aqueous solution by a low-cost activated carbon prepared from Mahagoni (*Swietenia mahagoni*) bark. *Pollution* **6** (1), 171–184. https://doi.org/10.22059/poll.2019.289061.679.

Hu, B., Huang, C., Li, X., Sheng, G., Li, H., Ren, X. & Huang, Y. 2017 Macroscopic and spectroscopic insights into the mutual interaction of activated carbon oxide, Cu (II), and Mg/Al layered double hydroxides. *Chemical Engineering Journal* **313**, 527–534. https://doi.org/10.1016/j.cej.2016.12.102.

Karri, R. R. & Sahu, J. N. 2018 Modeling and optimization by particle swarm embedded neural network for adsorption of zinc (II) by palm kernel shell based activated carbon from aqueous environment. *Journal of Environmental Management* **206**, 178–191. https://doi.org/10.1016/j.jenvman.2017.10.026.

Khajeh, M., Moghaddam, M. G. & Shakeri, M. 2012 Application of artificial neural network in predicting the extraction yield of essential oils of *Diplotaenia cachrydifolia* by supercritical fluid extraction. *The Journal of Supercritical Fluids* **69**, 91–96. https://doi.org/10.1016/j.supflu.2012.05.006.

Khan, T., Binti Abd Manan, T. S., Isa, M. H., Ghanim, A. A., Beddu, S., Jusoh, H. & Jami, M. S. 2020 Modeling of Cu (II) adsorption from an aqueous solution using an artificial neural network (ANN). *Molecules* **25** (14), 3263. https://doi.org/10.3390/molecules25143263.

Kousha, M., Tavakoli, S., Daneshvar, E., Vazirzadeh, A. & Bhatnagar, A. 2015 Central composite design optimization of Acid Blue 25 dye biosorption using shrimp shell biomass. *Journal of Molecular Liquids* **207**, 266–273. https://doi.org/10.1016/j.molliq.2015.03.046.

Lemessa, G., Chebude, Y. & Alemayehu, E. 2023 Adsorptive removal of Cr (VI) from wastewater using magnetite–diatomite nanocomposite. *AQUA – Water Infrastructure, Ecosystems and Society* **72** (12), 2239–2261.

Mahmood, T., Saddique, M. T., Naeem, A., Westerhoff, P., Mustafa, S. & Alum, A. 2011 Comparison of different methods for the point of zero charge determination of NiO. *Industrial & Engineering Chemistry Research* **50** (17), 10017–10023.

Mallakpour, S. & Behranvand, V. 2016 Manufacture and characterization of nanocomposite materials obtained from incorporation of d-glucose functionalized MWCNTs into the recycled poly (ethylene terephthalate). *Designed Monomers and Polymers* **19** (4), 283–289. https://doi.org/10.1080/15685551.2015.1136533.

Mouni, L., Belkhiri, L., Bollinger, J. C., Bouzaza, A., Assadi, A., Tirri, A. & Remini, H. 2018 Removal of Methylene Blue from aqueous solutions by adsorption on Kaolin: Kinetic and equilibrium studies. *Applied Clay Science* **153**, 38–45. https://doi.org/10.1016/j.clay.2017.11.034.

Musa, M. A., Chowdhury, S., Biswas, S., Alam, S. N., Parvin, S. & Sattar, M. A. 2023 Removal of aqueous methylene blue dye over *Vallisneria natans* biosorbent using artificial neural network and statistical response surface methodology analysis. *Journal of Molecular Liquids* **393**, 123624. https://doi.org/10.1016/j.molliq.2023.123624.

Nair, A. T. & Ahammed, M. M. 2014 Coagulant recovery from water treatment plant sludge and reuse in post-treatment of UASB reactor effluent treating municipal wastewater. *Environmental Science and Pollution Research* **21**, 10407–10418. https://doi.org/10.1007/s11356-014-2900-1.

Pereira, J. E., Silva, A. J., Nascimento, P. F., Ferreira, R. L. & Barros Neto, E. L. 2020 Carnauba straw powder treated with bentonite for copper adsorption in aqueous solution: Isothermal, kinetic and thermodynamic study. *Water Science & Technology* **82** (10), 2178–2192. https://doi.org/10.2166/wst.2020.491.

Rahmawati, I., Priyanto, A., Darsono, T. & Aji, M. P. 2019 The adsorption of dye waste using black carbon from polyethylene terephthalate (PET) plastic bottle waste. *Journal of Physics: Conference Series* **1321** (2), 022011. http://dx.doi.org/10.1088/1742-6596/1321/2/022011.

Renu, Agarwal, M. & Singh, K. 2018 Removal of copper, cadmium, and chromium from wastewater by modified wheat bran using Box–Behnken design: Kinetics and isotherm. *Separation Science and Technology* **53** (10), 1476–1489. https://doi.org/10.1080/01496395.2017.1417316.

Rouniasi, N., Monavvari, S. M., Abdoli, M. A., Baghdadi, M. & Karbassi, A. R. 2018 Optimization process for the removal of heavy metals from aqueous solution using activated carbon oxide nanosheets and response surface methodology. *Applied Ecology and Environmental Research* **16** (5), 6709–6729. http://dx.doi.org/10.15666/aeer/1605_67096729.

Saha, B. & Ghoshal, A. K. 2005 Thermal degradation kinetics of poly (ethylene terephthalate) from waste soft drinks bottles. *Chemical Engineering Journal* **111** (1), 39–43. https://doi.org/10.1016/j.cej.2005.04.018.

Sahmoune, M. N. 2019 Evaluation of thermodynamic parameters for adsorption of heavy metals by green adsorbents. *Environmental Chemistry Letters* **17** (2), 697–704. https://doi.org/10.1007/s10311-018-00819-z.

Wang, X. S. & Qin, Y. 2005 Equilibrium sorption isotherms for of Cu^{2+} on rice bran. *Process Biochemistry* **40** (2), 677–680. https://doi.org/10.1016/j.procbio.2004.01.043.

Zaman, S., Mehrab, M. N., Islam, M. S., Ghosh, G. C. & Chakraborty, T. K. 2021 Hen feather: A bio-waste material for adsorptive removal of methyl red dye from aqueous solutions. *H2Open Journal* **4** (1), 291–301. https://doi.org/10.2166/h2oj.2021.123.

Zaman, S., Biswas, P., Zaman, R., Islam, M. S., Mehrab, M. N., Ghosh, G. C. & Chakraborty, T. K. 2022 Jute (*Corchorus olitorius*) stick charcoal: A potential bioadsorbent for the removal of Cr (VI) from an aqueous solution. *H_2Open Journal* **5** (4), 656–669. https://doi.org/10.2166/h2oj.2022.027.

First received 6 September 2023; accepted in revised form 28 February 2024. Available online 11 March 2024